Model for the interpretation of hyperspectral remote-sensing reflectance

Zhongping Lee, Kendall L. Carder, Steve K. Hawes, Robert G. Steward, Thomas G. Peacock, and Curtiss O. Davis

Remote-sensing reflectance is easier to interpret for the open ocean than for coastal regions because the optical signals are highly coupled to the phytoplankton (e.g., chlorophyll) concentrations. For estuarine or coastal waters, variable terrigenous colored dissolved organic matter (CDOM), suspended sediments, and bottom reflectance, all factors that do not covary with the pigment concentration, confound data interpretation. In this research, remote-sensing reflectance models are suggested for coastal waters, to which contributions that are due to bottom reflectance, CDOM fluorescence, and water Raman scattering are included. Through the use of two parameters to model the combination of the backscattering coefficient and the Q factor, excellent agreement was achieved between the measured and modeled remote-sensing reflectance for waters from the West Florida Shelf to the Mississippi River plume. These waters cover a range of chlorophyll of 0.2–40 mg/m^3 and gelbstoff absorption at 440 nm from 0.02–0.4 m^{-1}. Data with a spectral resolution of 10 nm or better, which is consistent with that provided by the airborne visible and infrared imaging spectrometer (AVIRIS) and spacecraft spectrometers, were used in the model evaluation.

Introduction

The use of the power law of spectral-radiance ratios[1,2] to measure pigment concentrations requires that the water-leaving radiance be largely determined by variations in the pigment concentration, with all other optical constituents covarying with this quantity. The method works quite well for the open ocean, or case 1 waters,[3] in part because the water-leaving radiance of open ocean waters is hardly affected by bottom reflectance, land runoff, or suspended sediments. Although aeolian dust may be carried by winds to the open ocean,[4] the dominant effect of the particulates may still derive from phytoplankton.[5]

The power-law approach can be much less accurate for estuarine and coastal areas,[6] however, because many of the optical constituents are independent of phytoplankton concentrations. In these areas, the water-leaving radiance includes not only parts that are due to elastic scattering by water molecules, phytoplankton detritus, suspended particulates, and bottom reflectance, but also parts that are due to inelastic scattering of colored dissolved organic matter (CDOM) fluorescence and water Raman scattering. Thus, changes in ocean color resulting from suspended sediments or dissolved organic matter may be falsely interpreted as changes in pigment concentration.[6,7]

An approach to address these problems is to measure the light field and analytically separate the different spectral contributors. Optical models have been developed for the subsurface irradiance reflectance,[7,8] but satellites measure the radiance leaving the water surface. The water-leaving radiance is governed by two distinct parts: the solar input and in-water properties. When the remote-sensing reflectance (R_{rs}) is defined as the ratio of the water-leaving radiance $L_w(\lambda)$ to the above-surface downwelling irradiance $E_d(0^+, \lambda)$, R_{rs} will be independent of the intensity of the solar input. Models have been suggested by Carder and Steward,[9] Gordon *et al.*,[10] and Peacock *et al.*[11] to explain the measured R_{rs}, but in these works no contributions from CDOM fluorescence, water Raman reflectance, or bottom reflectance were included. Also, in these works[9,11] an arbitrary Q factor[12] was used.

For water-depth measurements[13,14] or bottom-

C. O. Davis is with the Jet Propulsion Laboratory, California Institute of Technology, 4800 Oak Grove Boulevard, Pasadena, California 91109; the other authors are with the Department of Marine Science, University of South Florida, 140 Seventh Avenue South, St. Petersburg, Florida 33701.

Received 29 December 1992; revised manuscript received 31 January 1994

0003-6935/94/245721-12$06.00/0.

feature mapping,[15] the diffuse attenuation coefficient[14] or an unclear effective attenuation coefficient[15] is usually used. For improvement of the interpretation of such measurements, an explicit expression is necessary for attenuation of the reflectance term that represents bottom reflectance. In this study, hyperspectral remote-sensing reflectance for waters from the West Florida Shelf to the Mississippi River plume was measured and modeled with a derived Q factor and the addition of bottom reflectance, CDOM fluorescence, and water Raman scattering.

Theory

The upwelling radiance leaving the ocean is a complicated mix of signals caused by many components. The major contributions arise from the following: absorption by molecules and particulates, elastic scattering by molecules and particulates, and bottom reflectance in shallow waters. Inelastic scattering processes (e.g., water Raman scattering and fluorescence of CDOM, chlorophyll, and phycoerythrin) are also contributors. Works by Carder and Steward[9] and Gordon[16] dealing with chlorophyll a (chl a) fluorescence have been reported, but, because the fluorescence efficiency varies by an order of magnitude,[9] this term is not considered in the present model. As peak chlorophyll fluorescence occurs in a narrow band centered around 685 nm,[17] its absence from the model is clearly seen when one compares values of measured and modeled R_{rs} (685) at higher chlorophyll concentrations. Perturbations between modeled and measured curves at ~580 nm and ~685 nm will be considered in the discussion relative to fluorescence that results from phycoerythrin and chl a, respectively.

It is assumed that the water-leaving radiance $L_w(\lambda)$ is dominated by the following four components: elastic scattering from molecules and particles $L_w{}^w(\lambda)$, bottom reflectance $L_w{}^b(\lambda)$, CDOM fluorescence $L_w{}^f(\lambda)$, and water Raman scattering $L_w{}^R(\lambda)$. It is also assumed that to the first order (single scattering and quasi-single scattering[18]) the water-leaving radiance can be expressed as

$$L_w(\lambda) = L_w{}^w(\lambda) + L_w{}^b(\lambda) + L_w{}^f(\lambda) + L_w{}^R(\lambda). \quad (1)$$

The symbols and definitions used in this paper are summarized in Table 1. Wavelength dependence is included here, but for convenience it is not included in the following discussions except when necessary for clarity.

Remote-sensing reflectance is defined as

$$R_{rs} = \frac{L_w}{E_d(0^+)}. \quad (2)$$

Breaking this equation into contributions from the various mechanisms listed in Eq. (1), we have

$$R_{rs} = R_{rs}{}^w + R_{rs}{}^b + R_{rs}{}^f + R_{rs}{}^R. \quad (3)$$

In the interpretation of the measured R_{rs} on the left side of Eq. (3), each component on the right side of Eq. (3) is expressed by the optical properties of the water.

A. Remote-Sensing Reflectance of the Water Column $R_{rs}{}^w$

For a homogeneous water body consider a wavelength-independent factor I as the influence of the air–sea interface on water-leaving radiance. Then the $R_{rs}{}^w$, which is due to eleastic scattering in the water column, can be described in terms of values just below the interface as

$$R_{rs}{}^w = I\frac{L_u{}^w(0^-)}{E_d(0^-)}, \quad (4)$$

where $I = t_+t_-/n^2$. For a zenith Sun, a nadir-viewing instrument, and a calm surface, $t \approx 0.98$ and $I \approx 0.533$ (Ref. 12) because n (1.341) varies only slightly when the salinity changes.[19] For larger solar zenith angles and foam-covered seas, t will be lower.[12] In our work, we specifically avoid foam-covered seas.

The subsurface-irradiance reflectance from the water column R^w is defined as the ratio of the subsurface upwelling irradiance $E_u{}^w(0^-)$ to the subsurface downwelling irradiance $E_d(0^-)$ by

$$R^w = \frac{E_u{}^w(0^-)}{E_d(0^-)}, \quad (5)$$

and Austin[12] has related $E_u{}^w(0^-)$ and $L_u{}^w(0^-)$ through the Q factor by

$$Q = \frac{E_u{}^w(0^-)}{L_u{}^w(0^-)}, \quad (6)$$

so $R_{rs}{}^w$ can be expressed as

$$R_{rs}{}^w = \frac{I}{Q}R^w. \quad (7)$$

For irradiance reflectance R^w, Gordon *et al.*[20] developed a series relation with the Monte-Carlo method by

$$R^w = \sum_{m=0}^{3} r_m\left(\frac{b_b}{a+b_b}\right)^m. \quad (8)$$

This equation was simplified[21,22] to

$$R^w \approx 0.33\frac{b_b}{a}, \quad (9)$$

for values of b_b/a up to ~0.25. The constant 0.33 actually varies slightly with the solar zenith angle.[23,24] Because this paper deals with remote-sensing reflectance, which is less influenced by the fraction of forward scatter that upwells at solar zenith angle $>0°$, R_{rs} is not as sensitive to the Sun angle, as is irradiance reflectance. Thus, we retain 0.33 as a

Table 1. Definitions and Units of Variables[a]

Variable	Units[a]	Definition
a	m^{-1}	Total absorption coefficient: $a_w + a_g + a_p$
a_g	m^{-1}	Gelbstoff-absorption coefficient
a_p	m^{-1}	Particle-absorption coefficient
a_w	m^{-1}	Pure water absorption coefficient
b	m^{-1}	Scattering coefficient
b_b	m^{-1}	Backscattering coefficient
b_{bm}	m^{-1}	Backscattering coefficient of molecules
b_{bp}	m^{-1}	Backscattering coefficient of particles
b_R	m^{-1}	Water Raman scattering coefficient
c	m^{-1}	Beam attenuation coefficient: $a + b$
$D_d(0)$		Downwelling distribution function just below the surface
$\{D_d\}$		Vertically averaged downwelling distribution function
E_d	$W\ m^{-2}$	Downwelling irradiance
E_o	$W\ m^{-2}$	Total scalar irradiance
E_{od}	$W\ m^{-2}$	Downwelling scalar irradiance
E_{ou}	$W\ m^{-2}$	Upwelling scalar irradiance
$E_u{}^w$	$W\ m^{-2}$	Upwelling irradiance from water column only
H	m	Water depth
k	m^{-1}	Radiance attenuation coefficient
j	rad	Subsurface solar zenith angle
K_d	m^{-1}	Downwelling diffuse attenuation coefficient
K_u	m^{-1}	Upwelling diffuse attenuation coefficient
$L_u{}^w$	$W\ m^{-2}\ sr^{-1}$	Upwelling radiance from water column (elastic only)
L_w	$W\ m^{-2}\ sr^{-1}$	Total water-leaving radiance
$L_w{}^b$	$W\ m^{-2}\ sr^{-1}$	Water-leaving radiance from bottom reflectance
$L_w{}^f$	$W\ m^{-2}\ sr^{-1}$	Water-leaving radiance from CDOM fluorescence
$L_w{}^R$	$W\ m^{-2}\ sr^{-1}$	Water-leaving radiance from water Raman scattering
$L_w{}^w$	$W\ m^{-2}\ sr^{-1}$	Water leaving radiance from water column (elastic only)
n		Refractive index of water
Q	sr	Ratio of irradiance to radiance
R		Irradiance reflectance
R_{rs}	sr^{-1}	Remote-sensing reflectance
$R_{rs}{}^b$	sr^{-1}	Remote-sensing reflectance from bottom reflectance
$R_{rs}{}^f$	sr^{-1}	Remote-sensing reflectance from CDOM fluorescence
$R_{rs}{}^{fR}$	sr^{-1}	Sum of $R_{rs}{}^f$ and $R_{rs}{}^R$
$R_{rs}{}^R$	sr^{-1}	Remote-sensing reflectance from water Raman
$R_{rs}{}^w$	sr^{-1}	Remote-sensing reflectance from water column (elastic only)
R^w		Irradiance reflectance from water column (elastic only)
t_+		Air–sea surface transmittance for upwelling radiant flux
t_-		Air-sea surface transmittance for downwelling radiant flux
T_{ie}	$W\ sr^{-1}$	Intensity of the inelastically scattered light
y_b		Exponent for particle backscattering coefficient
y_Q		Exponent for particle Q factor
α	rad	Scattering angle
β	$m^{-1}\ sr^{-1}$	Volume scattering function
ϕ	rad	Azimuth angle
γ		Irradiance ratio of skylight to sunlight
κ	m^{-1}	Quasi-diffuse attenuation coefficient: $a + b_b$
λ_x	nm	Excitation wavelength for inelastic scattering
η		Quantum efficiency of CDOM fluorescence
ψ	$m^{-1}\ nm^{-1}$	Inelastic scattering coefficient
ρ		Bottom albedo
Θ	rad	Zenith angle

[a]Blank entries denote dimensionless quantities.

constant and embed any sun-angle influence within the Q factor expression (see Appendix A).

The total backscattering coefficient b_b includes two components: backscattering by molecules b_{bm} and particulates b_{bp}. The total absorption coefficient a includes contributions that are due to pure seawater absorption a_w, gelbstoff or CDOM absorption a_g, and particulate absorption a_p. Inserting these into Eq. (9) and taking $I \approx 0.533$, we can write $R_{rs}{}^w$ as

$$R_{rs}{}^w \approx \frac{0.176}{a_w + a_g + a_p} \frac{b_{bm} + b_{bp}}{Q}. \quad (10)$$

Eq. (10) pertains to optically deep water. When optically shallow water is encountered, scattering media and backscattered signals are reduced because

of the short water column. We consider that the subsurface E_u^w consists of two parts coming from two layers: one from the layer above the bottom and one from the layer below the bottom. Then the subsurface E_u^w coming only from the upper layer can be obtained by a reduction of the optically deep expression by an amount equivalent to the contribution of the missing water column below depth H. Thus for shallow waters with depth H and a totally absorbing bottom, R_{rs}^w is approximated by

$$R_{rs}^w \approx \frac{0.176\, b_b}{a\, Q}\left\{1 - \exp\left[-\int_0^H (K_d + K_u)dz\right]\right\}, \quad (11)$$

where z is positive downward from the surface.

If we define the quasi-diffuse attenuation coefficient as $\kappa = a + b_b$, then $K_d \approx D_d\kappa$ and $K_u \approx D_u\kappa$[20]. D_d and D_u are the distribution functions for the downwelling and upwelling light fields, and $D_u/D_d \approx 2$ according to Gordon *et al.*[20] Thus

$$R_{rs}^w \approx \frac{0.176\, b_b}{a\, Q}[1 - \exp[-3\{D_d\}\kappa H], \quad (12)$$

where $\{D_d\}$ is the vertically averaged downwelling distribution function and $\{D_d\} \approx 1.08D_d(0)$.[25] $D_d(0)$ is the downwelling distribution function just beneath the surface, and $D_d(0) \approx 1/\cos(j)$, with an error of less than 3%.[25]

B. Remote-Sensing Reflectance Resulting from Bottom Reflectance R_{rs}^b

Assume that the bottom is a Lambertian reflector with bottom albedo ρ, then R_{rs}^b can be approximated as

$$R_{rs}^b \approx \frac{0.533}{\pi}\rho \exp[-(\{D_d\}\kappa + k)H], \quad (13)$$

where k is the effective attenuation coefficient for the radiance from an extended Lambertian source. How k relates to the quasi-diffuse attenuation coefficient κ is not well understood. Heuristically, it should be a value between the beam attenuation coefficient c and the quasi-diffuse attenuation coefficient κ. Taken from the Monte-Carlo simulations for a totally diffuse light source,[25] k is approximately 1.4κ to 1.7κ for κH in the range of 0.5–4.0. As an average in this work, $k = 1.5\kappa$, as is used by Marshall and Smith.[26] Then Eq. (13) becomes

$$R_{rs}^b \approx 0.17\rho \exp[-(1.5 + \{D_d\})\kappa H]. \quad (14)$$

C. Remote-Sensing Reflectance Resulting from CDOM Fluorescence and Water Raman Scattering R_{rs}^f and R_{rs}^R

In general, these terms are due to inelastic scattering (indicated by the subscript ie) by CDOM molecules and water molecules. We defne the volume scattering function for inelastic scattering as

$$\beta_{ie}(\alpha, \lambda_x, \lambda) = \frac{T_{ie}(\alpha, \lambda)}{E(\lambda_x)dV}, \quad (15)$$

where $T_{ie}(\alpha, \lambda)$ is the intensity of the inelastically scattered light at scattering angle α, dV is the scattering volume, $E(\lambda_x)$ is the irradiance of the excitation beam, and α is the angle between the excitation beam and the output photon directions.

If β_{ie} is considered to be isotropic, then remote-sensing reflectance resulting from CDOM fluorescence and water Raman can be expressed (see Appendix B for details) as

$$R_{rs}^f \approx 0.072 \int_{\lambda_x} \eta(\lambda_x)\frac{\lambda_x}{\lambda}\frac{a_g(\lambda_x)E_d(0^-, \lambda_x)}{[2a(\lambda) + a(\lambda_x)]E_d(0^-, \lambda)} \times \frac{\exp\left[-s\left(\ln\frac{\lambda - \lambda_0}{\sigma}\right)^2\right]}{A} d\lambda_x, \quad (16)$$

$$R_{rs}^R \approx 0.072\frac{b_R(\lambda_x)E_d(0^-, \lambda_x)}{[2a(\lambda) + a(\lambda_x)]E_d(0^-, \lambda)}. \quad (17)$$

Field Measurements

From 1990 to 1993, measurements of optical properties for case 1 and case 2 waters, which include waters from the West Florida Shelf to the mouth of Mississippi River, were taken. Case 2 waters are those that contain optical materials that are not derived from phytoplankton, in addition to phytoplankton and phytoplankton-derived materials.[3] Table 2 summarizes the field data for selected stations. Figure 1 shows the station locations in the Gulf of Mexico. For each station, remote-sensing reflectance R_{rs} and surface-water particulate absorption a_p were measured. For the 1993 stations, a long-path (50 or 100 cm) spectrophotometer was used to measure a_g.

For R_{rs} we directly measured the upwelling radiance above the sea surface and downwelling sky radiance using a Spectron Engineering spectral radiometer (Model SE–590) following the method of Carder *et al.*[27] We measured downwelling irradiance above the sea surface with the SE–590 by viewing a Spectralon diffuse-reflection calibration panel. Remote-sensing reflectance values were determined by removal of the reflected skylight from the upwelling-radiance values[9,27] and division of the result by the downwelling-irradiance values. For each station, three sets of measurements were taken, and an averaged R_{rs} spectrum was derived, with coefficients of variation much less than 5%.

For a_p, we measured a surface-water sample immediately after its collection following the method developed by Mitchell and Kiefer.[28] Briefly, for each water sample, ~1000 mL (with variations according to the clarity of the water sample) were filtered through Whatman-type GF/F glass-fiber filters. Hyperspectral optical densities of the sample pad and

Table 2. Station Locations and Water Depth

Station	Latitude	Longitude	Time	Date	Bottom Depth	Mod. Bottom Depth
ST01	27°27′ N	82°55′ W	10.5[a]	4 Mar 1990	~14 m	13.7 m
ST02	27°20′ N	83°03′ W	13.0[a]	4 Mar 1990	~25 m	25 m
ST03	27°12′ N	83°11′ W	14.9[a]	4 Mar 1990	~35 m	36 m
ST08	28°48′ N	91°30′ W	08.5[b]	12 Apr 1993	OD[d]	OD
ST10	28°15′ N	91°30′ W	14.0[b]	12 Apr 1993	OD	OD
ST27	29°32′ N	85°47′ W	09.2[b]	19 Apr 1993	OD	OD
ST12	28°52′ N	89°33′ W	10.8[c]	5 Jun 1993	OD	OD
ST14	28°48′ N	90°02′ W	16.1[c]	5 Jun 1993	OD	OD
ST19	27°34′ N	83°20′ W	09.5[c]	8 Jun 1993	~33 m	35 m

[a]Eastern standard time.
[b]Central daylight time.
[c]Eastern daylight time.
[d]Water is optically deep (OD).

a wet blank pad were measured with the Spectron. The optical-path-elongation factor β was calculated with Eq. (2) in Bricaud and Stramski.[29] The optical density measurements were repeated three times with no significant variation noted among them.

At the 1990 stations, gelbstoff absorption a_g was derived from surface-layer K_d values determined with a Biospherical Instruments MER–1048, through the use of the expression $a_g = K_d \cos(j) - a_w - a_p$. At the 1993 stations, a_g was measured with 50-cm or 100-cm path-length instruments, respectively, after the sample was filtered through 0.2-μm pore-diameter Gelman Supor-200 filters.

Model

For the modeling of measured R_{rs} spectra, values for a_w and b_{bm} were already known,[30] a_p was measured, and a_g was measured or derived from K_d spectra. What needs to be considered is how Q, b_{bp}, ρ, H, η, s, λ_0, and σ change for different environments.

$R_{rs}{}^R$

Because Raman is a type of molecular scattering, $b_R(\lambda_x)$ is considered to have a wavelength dependence similar to that of the water-molecule scattering coefficient,[31] i.e., a function of λ^{-4}. Because $b_R(488) = 2.6 \times 10^{-4}\ m^{-1}$ (Marshall and Smith[26]), thus $b_R(\lambda_x) = 2.6 \times 10^{-4}(488/\lambda_x)^4$, and the frequency shift for water Raman scattering was fixed at 3350 cm^{-1} as an average from Collins *et al.*[32] The incoming, total downwelling-irradiance spectrum was measured with a Licor 1800 spectral irradiance meter[27] from 300–850 nm. Then it is straightforward to calculate $R_{rs}{}^R$ with Eq. (17) when the total absorption spectrum is known.

$R_{rs}{}^f$

As can be seen from Eq. (16), there are at least four variables [$\eta(\lambda_x)$, s, λ_0, and σ] needed to calculate the remote-sensing reflectance that results from CDOM

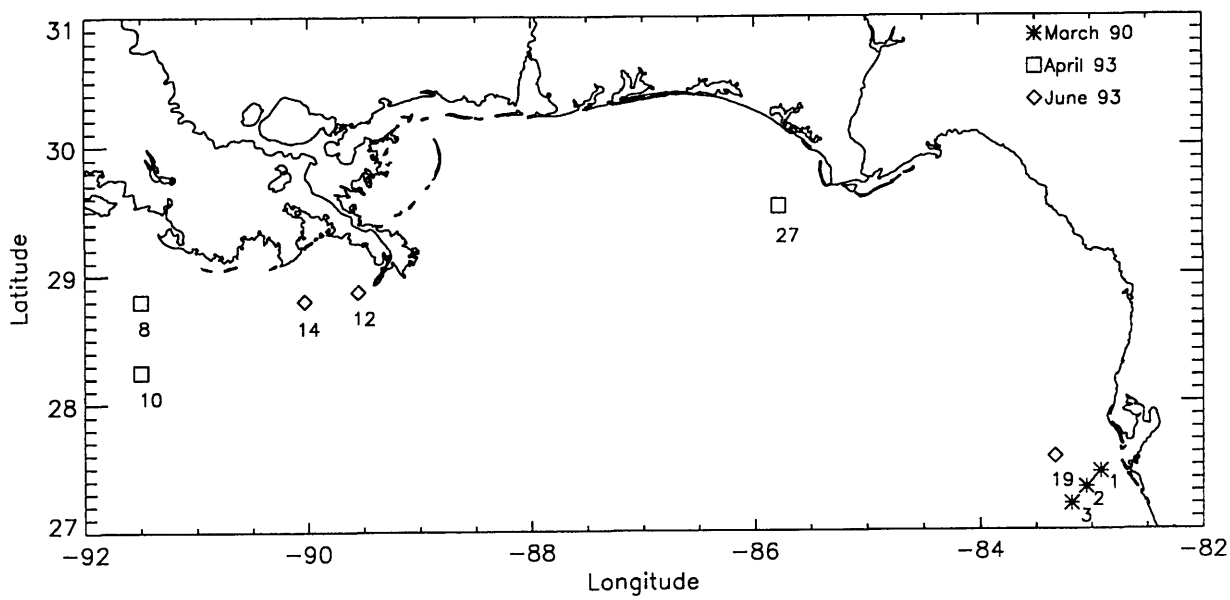

Fig. 1. Station locations in the Gulf of Mexico.

fluorescence when the total absorption coefficient is known. From lab measurements of CDOM fluorescence for the West Florida Shelf experiments,[33] the quantum efficiency $\eta(\lambda_x)$ was between $\sim 0.5\%$ and $\sim 1.5\%$, and it was generally rather constant for different excitation wavelengths. For the log-normal expression in $R_{rs}f$, the shape factor s was 10, $\lambda_0 \sim (.95\lambda_x - 45)$, and $\sigma \sim (195 - \lambda_x/5)$, all of which were quite constant for the different stations.[33] Based on these measurements, $\eta = 1.0\%$ was used for all the stations except ST03, where $\eta = 1.5\%$ was measured. At ST12, ST14, and ST01 where significant terrigenous CDOM was present, $\eta = 0.5\%$ was used.

$R_{rs}{}^b$

This value depends not only on the optical properties of the water body, but also on the water depth and the bottom albedo. In the modeling work, the water depth was based on the Provisional Chart No. 1003[34] for the Gulf Coast, and the bottom albedo was based on earlier measurements of bottom samples from the region that had near-shore values of 0.1–0.2 (used for ST01) and offshore values from 0.4–0.5 (used for ST02 and ST03). Figure 7 (below) shows examples of those albedo spectra. The quasi-diffuse attenuation coefficient κ is assumed to be equal to the absorption a. For ST19, an albedo value of 0.1 is required, which suggests that the bottom might contain more heavy minerals or grass at that site. Direct bottom-albedo measurements are lacking at individual stations and are needed for a wide variety of bottom types.

$R_{rs}{}^w$

When using Eq. (10) to model the measured $R_{rs}{}^w$, we need to know a_w, a_g, a_p, b_{bm}, b_{bp}, and Q. Values of a_w and b_{bm} are already known.[30] When a_g and a_p are measured, only b_{bp} and Q for different water bodies and solar zenith angles are required. The particulate backscattering coefficient b_{bp} has been considered to be a spectral function of λ^{-1} for offshore waters or to be spectrally constant for near-shore waters.[11,35]

For the factor Q, however, only a few measurements exist, and its values have been reported from 3.2 to 12.[9] Q has been taken to be approximately 4.7 and spectrally constant from 440–550 nm,[36] although Kirk[37] gives Q as ~ 4.9, and Gordon *et al.*[10,20] suggest a value of ~ 3.4. For many studies, Q is often arbitrarily chosen as a spectral constant.[9,11,13] From measurements by Davis,[38] however, Carder *et al.*[6] found that Q is not spectrally constant for the 1990 stations, and there was a trend for Q to increase with wavelength (an inverse trend compared with b_{bp}). Recently, Morel and Gentili[39] published Monte-Carlo simulations of Q for a variety of water types, but they provide no explicit expression for Q as a function of a and b_b or β. So, for modeling $R_{rs}{}^w$ for a region where spectral b_{bp} and Q need to be considered, at least four parameters are needed based on Eq. (10): two for $b_{bp}(\lambda)$ and two for $Q(\lambda)$.

If we consider the upwelling radiance of the water column $L_u{}^w$ as consisting of two parts—one $L_u{}^m$ that is due to scattering by molecules and one $L_u{}^p$ that is due to scattering by particles—with the assumption that to the first order (for single scattering and quasi-single scattering[18]) the sum of $L_u{}^m$ and $L_u{}^p$ gives $L_u{}^w$, then Eq. (10) can be written as

$$R_{rs}{}^w \approx \frac{0.176}{a_w + a_g + a_p}\left(\frac{b_{bm}}{Q_m} + \frac{b_{bp}}{Q_p}\right), \tag{18}$$

in which Q_m and Q_p are the Q factors for molecules and particles, respectively, and are defined as

$$Q_m = \frac{E_u{}^m(0^-)}{L_u{}^m(0^-)}, \qquad Q_p = \frac{E_u{}^p(0^-)}{L_u{}^p(0^-)}. \tag{19}$$

For Q_m to the first order an estimate can be made based on the phase function and illumination geometry. For a given illumination geometry, the shape of the radiance distribution within the water is determined primarily by the volume scattering function through single scattering. For example, Gordon[25] suggested that a single-scattering approximation can be used to specify the variation of R with the solar zenith angle, and Kirk[22] used single scattering to describe the average cosine. We combined the approach used by Jerlov[40] to provide an estimation of radiance and irradiance with Sun angle and depth, Austin's definition of the Q factor,[12] and the volume scattering function of water molecules given by Morel[41] to calculate the Q_m for sunlight (see Appendix A for details). The results can be approximated with the following simple function:

$$Q_m{}^{sun}(j) \approx 5.92 - 3.05\cos(j). \tag{20}$$

With the assumption that the Q_m attributable to skylight is approximately 3.14, the effective Q_m for a mixture of sunlight and skylight is given by (Appendix A)

$$Q_m = \frac{1 + \gamma(\lambda)}{1 + \gamma(\lambda)\dfrac{Q_m{}^{sun}(j)}{3.14}}\, Q_m{}^{sun}(j), \tag{21}$$

if we define $\gamma(\lambda) = E_d{}^{sky}/E_d{}^{sun}$, and calculate $\gamma(\lambda)$ using the model developed by Gregg and Carder.[42] Model results of $Q_m{}^{sun}(j)$ centered around 3.3 for environments studied in this contribution and are shown in Table 3, and the calculated $Q_m{}^{sun}$ is consistent with Morel and Gentili's Monte-Carlo results.[39]

Because we know the volume scattering function for neither the total water sample nor the particles, b_{bp} and Q_p cannot be independently estimated. However, because b_{bp} has been considered a function of $b_{bp}(400)(400/\lambda)^{yb}$ as in Smith and Baker,[30] we may also consider Q_p to be a function of $Q_p(400)(\lambda/400)^{yQ}$.

Table 3. Parameters for Each Station[a]

Station	j	Q_m^{sun}	X	Y	$a_g(440)$	$a_p(440)$	$a_p^{mea}(440)$	[chl a] (mg/m^3)
ST01	35°	3.3	0.0090	1.5	0.082	0.040	0.045	1.05
ST02	26°	3.2	0.0020	2.4	0.042	0.036	0.035	0.61
ST03	27°	3.2	0.0010	2.4	0.034	0.028	0.026	0.70
ST08	43°	3.7	0.0062	0.3	0.31	0.28	0.295	
ST10	17°	3.0	0.0009	1.8	0.059	0.023	0.021	
ST27	36°	3.5	0.0011	1.7	0.078	0.029	0.034	
ST12	30°	3.3	0.0029	0	0.42	1.40	1.12	38.58
ST14	21°	3.1	0.0066	0	0.38	1.21	1.16	20.26
ST19	37°	3.5	0.00061	1.9	0.023	0.022	0.013	0.22

[a]Blank entries indicate that no data are available.

Then b_{bp}/Q_p can be combined and modeled as

$$\frac{b_{bp}}{Q_p} = \frac{b_{bp}(400)}{Q_p(400)}\left(\frac{400}{\lambda}\right)^{(y_b+y_Q)} = X\left(\frac{400}{\lambda}\right)^{Y}, \quad (22)$$

where X and Y are two unknowns determined for specific particulate suites and solar illumination situations if Eq. (18) is inverted.

After calculating $R_{rs}{}^R$, $R_{rs}{}^f$, and $R_{rs}{}^b$, only X and Y remain unknown. The modeled $R_{rs}{}^w$ and the residual of $R_{rs} - R_{rs}{}^R - R_{rs}{}^f - R_{rs}{}^b$ were matched to derive X and Y with a predictor–corrector approach to modeling, as in Carder and Steward.[9]

Results and Discussion

Using the methodology described above (see Model) we modeled R_{rs} for case 1 and case 2 waters, which include (1) the West Florida Shelf waters, with shallow, gelbstoff-rich coastal waters, and (2) Gulf of Mexico waters, with phytoplankton blooms in the Mississippi River plume ($S > 17\%$). As examples, Figs. 2–5 show the detailed model components for R_{rs}, and Fig. 6 shows the results of all the listed stations. Table 2 provides the station locations as well as the measured and modeled water depths of the shallow stations. Table 3 lists the model parameters j, Q_m^{sun}, X, Y, $a_g(440)$ and $a_p(440)$ along with the measured values of $a_p(440)$ and the chl a concentration values for each station. Table 4 details the fractional contributions that $R_{rs}{}^w$, $R_{rs}{}^R$, $R_{rs}{}^f$, and $R_{rs}{}^b$ make to the measured R_{rs} at 440 and 550 nm.

It can be seen from Figs. 2–6 that excellent fittings were achieved between the measured and modeled R_{rs} for all the stations except the spectral region near 685 nm, where chl a fluorescence is present in the field data. The overall averaged difference between the measured and modeled R_{rs} is 2%, which is well within the measurement accuracy. The a_p that is required by the model is within 15% of the measured a_p except near the Mississippi River at ST12 (25%), with the highest chl a concentration (38.6 mg/m^3). The average difference between the measured and required a_p is 8.9% (6.9% when ST12 is excluded). The maximum 15% or 25% difference can perhaps be explained by the accuracy involved in the method of a_p measurement because of the β factor, which varies significantly among species.[29] This may be especially important for ST12, which was near the Mississippi River mouth where the heavy load of sediments and minerals might cause additional uncertainty. Also, the influence of the horizontal and vertical structures of the waters increases for mesotrophic–eutrophic waters, so patchiness can affect accuracies in the more hypertrophic waters. Finally, the low signal obtained for the upwelling radiance measurements at

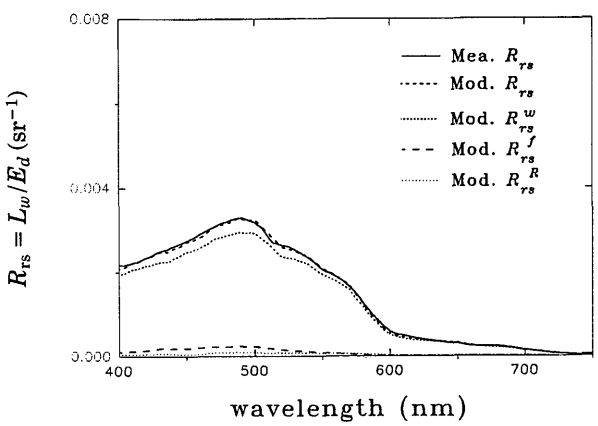

Fig. 2. Measured versus modeled R_{rs} for ST27.

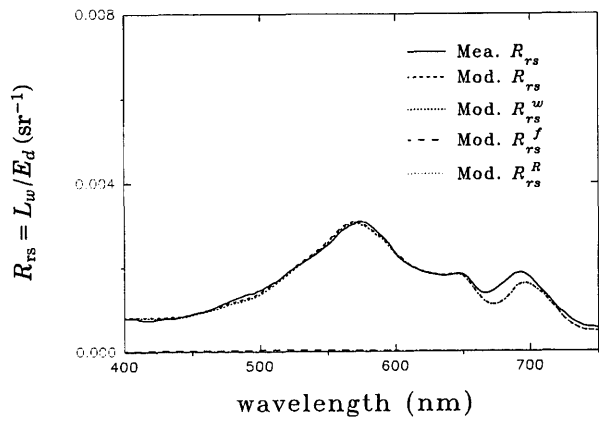

Fig. 3. Measured versus modeled R_{rs} for ST14.

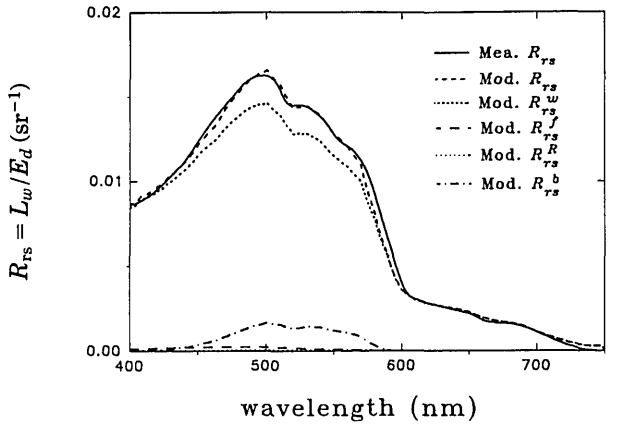

Fig. 4. Measured versus modeled R_{rs} for ST01.

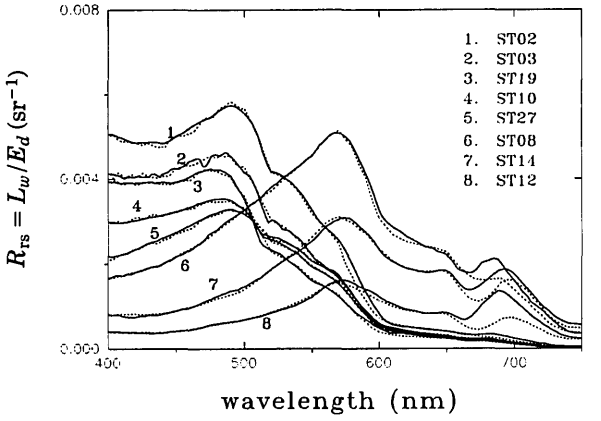

Fig. 6. Measured (solid curve) versus modeled (dashed curve) R_{rs} for all the stations except ST01.

ST12 made the R_{rs} calculation sensitive to corrections for reflected skylight.

From Table 3, the ratio of $a_g(440)$ to $a_p(440)$ is highly variable, with a range from ~0.3 to ~3.0, and the X value does not covary with the pigment concentration of chl a for the waters studied. This illustrates that the model works well over a wide range of conditions and also suggests why the power-law algorithm does not work well for coastal waters. The highest X value, 0.0090 m^{-1} sr^{-1}, was at the shallow, mesotrophic waters at ST01, which suggests a high influence of detritus and suspended sediments. Brisk northwesterly winds suspended sediments in the shoal regions to the east and north of the station, and sediment and detritus likely were transported by the ebb tidal currents from Tampa Bay to the study site.[27]

The Y values were generally within the range of 0–2.4 for the waters reported here. This range might be interpreted to be partially due to b_{bp} and partially due to Q_p. For the particle backscattering coefficient b_{bp} the wavelength exponent is in the range 0–3.0 for a range of particle sizes (e.g., bacteria,[43] phytoplankton cells,[44] and coccoliths[10]). From Eq. (22), if $Y = 2.4$ and $y_Q = 1.0$, then $y_b = 1.4$, which is within the 0–3.0 range reported elsewhere.

Model results at ST03 suggest relatively higher CDOM fluorescence and water Raman influences,

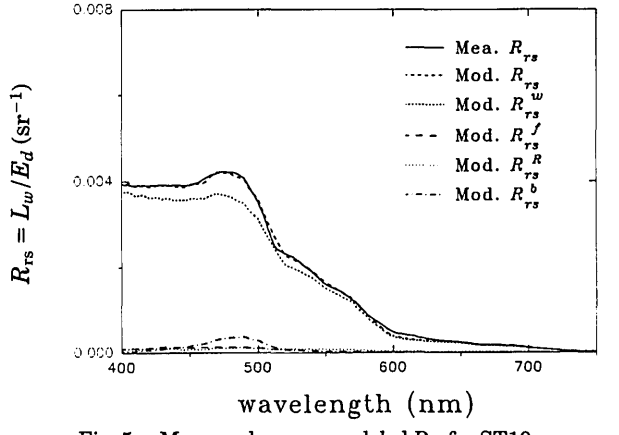

Fig. 5. Measured versus modeled R_{rs} for ST19.

because a higher η (1.5%) was encountered.[33] This value is ~3 times greater than the value suggested by Spitzer and Dirks[45] for terrigenous CDOM. If we exclude this station, more than 90% of the water-leaving radiance is accounted for by the sum of the elastic scattering from molecules, particles, and the bottom. This is consistent with the reports of Marshall and Smith[26] and Stavn,[46] because the waters studied in their reports were clearer. Water Raman scattering makes more of a contribution when the water is clear, and $R_{rs}{}^{fR}/R_{rs}$ will typically have a higher value at 550 nm than at 440 nm.

It is interesting that the ratio $R_{rs}(440)/R_{rs}(550)$ did not vary widely (within 15%) because of inelastic scattering (see Table 4). Among stations without bottom influence, differences in the ratio were within ~10%, which suggests the spectral-radiance ratio is effective for most deep waters without consideration of CDOM fluorescence and water Raman scattering. But it is obvious that as the bottom influence increases the usefulness of the power-law algorithm decreases. Also, the power-law algorithm cannot distinguish between the absorption of CDOM and that of pigments. Note also that $R_{rs}{}^{w}(490)/R_{rs}(490)$ values as low as 0.77 were determined (not explicitly shown), which suggests that great care must be taken when one is interpreting remote-sensing curves for the intermediate wavelength at shallow coastal stations.

At the optically shallow stations (ST01, ST02, ST03, and ST19), the model-derived depths were within approximately 10% of the chart depths without consideration of any tidal influence (typically < 0.5 m). This demonstrates a potential to use this model to survey, e.g., by aircraft overflights, dramatic changes in shelf bathymetry that can occur as a result of major storm.

For ST01, ST02, ST03, ST08, ST12, and ST14, the general agreement between the modeled and measured R_{rs} values are very good, with small differences near 580 nm, where the measured R_{rs} > modeled R_{rs}. Other than the modeling error, there are at least three possible reasons for this: (1) bottom-albedo uncertainty, (2) phycoerythrin fluorescence,[47] and (3)

Table 4. Optical Component Contributions[a] to R_{rs}

Station	R_{rs}^{w}/R_{rs} 440 nm	R_{rs}^{w}/R_{rs} 550 nm	R_{rs}^{fR}/R_{rs} 440 nm	R_{rs}^{fR}/R_{rs} 550 nm	R_{rs}^{b}/R_{rs} 440 nm	R_{rs}^{b}/R_{rs} 550 nm	$R_{rs}(440)/R_{rs}(550)$ Measured R_{rs}	$R_{rs}(440)/R_{rs}(550)$ Corrected R_{rs}
ST01	0.95	0.89	0.02	0.01	0.02	0.10	0.87	0.92
ST02	0.91	0.80	0.05	0.06	0.04	0.12	1.48	1.73
ST03	0.86	0.81	0.10	0.12	0.02	0.04	1.87	2.00
ST08	0.98	0.99	0.03	0.02			0.49	0.48
ST10	0.92	0.93	0.08	0.07			1.64	1.60
ST27	0.90	0.94	0.08	0.07			1.34	1.29
ST12	0.90	0.97	0.09	0.03			0.31	0.27
ST14	0.97	0.99	0.03	0.01			0.32	0.30
ST19	0.92	0.92	0.06	0.07	0.03	0.01	2.46	2.36

[a] $R_{rs}^{fR} = R_{rs}^{f} + R_{rs}^{R}$ and corrected R_{rs} = measured $R_{rs} - R_{rs}^{fR} - R_{rs}^{b}$. Blank entries indicate that no data are available.

water-absorption coefficient uncertainty.[11] A spectrally constant bottom albedo was used for the shallow stations. Earlier measurements of bottom albedo (Fig. 7) did display some spectral dependence, but these types of changes could not provide the sharp increase and then decrease with wavelength in R_{rs} required for the measured and modeled R_{rs} curves to converge. Also, there was no bottom contribution to R_{rs} at ST08, ST12, or ST14. More realistic explanations include the lack of a term for phycoerythrin fluorescence or the differences between the water-absorption coefficients in this spectral region reported by Smith and Baker[30] and Tam and Patel.[48] Further study is required to resolve this issue. The differences between the measured and modeled R_{rs} curves near 685 nm are expected because no term is included in the model to describe the chl *a* fluorescence.

Summary

Contributions to the water-leaving radiance spectra for a variety of waters were attributed to elastic shattering by water molecules, suspended particles, and bottom reflectance, and to inelastic scattering by water Raman and CDOM (or gelbstoff) fluorescence. Inelastic scattering by pigments was not considered. For optically deep water, remote-sensing reflectance

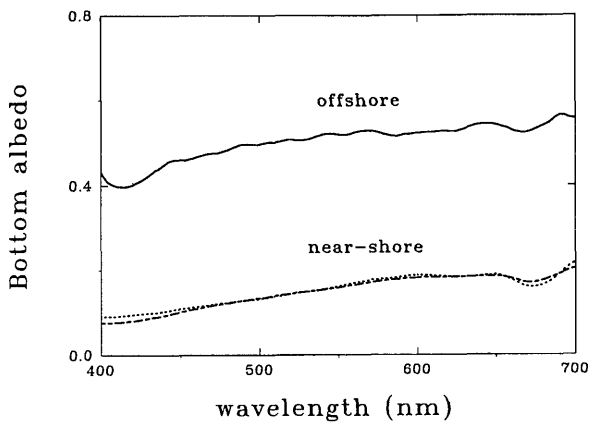

Fig. 7. Bottom-albedo spectra for near-shore (dashed curve) and offshore (solid curve) sediments, measured for samples on earlier cruises and retrieved from a grab sampler or by divers.

of the water-column part (elastic scattering only) R_{rs}^{w} was simulated as follows:

$$R_{rs}^{w} \approx \frac{0.176}{a_w + a_g + a_p}\left[\frac{b_{bm}}{Q_m} + X\left(\frac{400}{\lambda}\right)^{Y}\right], \quad (23)$$

where b_{bm} is known, Q_m can be estimated, and X and Y are spectral constants. Q_m^{sun} averaged approximately 3.3, and Y was less than 2.4 for the waters considered. For optically shallow waters, the expression for bottom reflectance

$$R_{rs}^{b} \approx 0.17\rho \exp[-(1.5 + \{D_d\})aH], \quad (24)$$

works well for the shallow waters that we considered. Together, the water-column term and the bottom-reflectance term accounted for more than 90% of the total remote-sensing reflectance.

Close agreement between modeled and measured R_{rs} was achieved for all stations when all scattering mechanisms mentioned above (both elastic and inelastic) were included. The ratio $a_g(440)/a_p(440)$ covered a range from ~0.3 to ~3.0, which indicates the wide usefulness of the model. For contributions other than those from the water column, as much as 23% of $R_{rs}(490)$ is attributable to water Raman, CDOM fluorescence, and bottom reflectance for an optically shallow (25 m) station. For the power law of spectral radiance ratio, most error comes from reflected bottom radiance for coastal waters. For most deep waters, the power-law algorithm can be used without the correction of CDOM fluorescence and water Raman with little error if the optical properties covary with chlorophyll, because the inelastic effects cover the whole range from 400–600 nm with generally less than 10% contributions to the water-leaving radiance.

The a_p required by the model is generally within 15% of the measured a_p, with an average difference of 8.9% (6.9% when ST12 is excluded). This suggests a method to remotely measure the pigment- and gelbstoff-absorption coefficients, although derivation of chl *a* concentration will depend on knowledge of the specific absorption coefficient for a region. Also the model-derived bottom depths for optically shallow waters are within 10% of the chart depths, which

suggests its possible use to remotely measure bottom depth for the shelf waters.

Appendix A: Simple Estimation of $Q_m(j, \lambda)$

If we follow the method described by Jerlov,[40] the subsurface upwelling irradiance $E_u^{\text{sun}}(0^-, \lambda)$ caused by subsurface sunlight $E_d^{\text{sun}}(0^-, \lambda)$ can be obtained for single scattering and quasi-single scattering[18] by

$$E_u^{\text{sun}}(0^-, \lambda) = E_d^{\text{sun}}(0^-, \lambda)\frac{\sec(j)\exp[-cz\sec(j)]}{c} \times \int_0^{2\pi}\int_{\pi/2}^{\pi}\frac{\beta(\alpha, \lambda)\sin(\theta)}{\sec(\theta) + \sec(j)}\,d\theta d\phi, \quad \text{(A1)}$$

where α is the scattering angle, Θ is the zenith angle, ϕ is the azimuth angle, and

$$\cos(\alpha) = -\cos(\Theta)\cos(j) + \sin(\Theta)\sin(j)\cos(\phi).$$

The upwelling radiance from the nadir resulting from this situation is

$$L_u^{\text{sun}}(0^-, \lambda) = E_d^{\text{sun}}(0^-, \lambda)\frac{\beta(\pi - j, \lambda)}{c[\cos(j) + 1]} \times \exp[-cz\sec(j)]. \quad \text{(A2)}$$

Recalling Austin's definition[12] for the Q factor E_u/L_u, we get

$$Q_m^{\text{sun}}(j, \lambda) = \frac{\int_0^{2\pi}\int_{\pi/2}^{\pi}\frac{\beta(\alpha, \lambda)}{\cos(j) + \cos(\theta)}\cos(\theta)\sin(\theta)d\theta d\phi}{\frac{\beta(\pi - j, \lambda)}{\cos(j) + 1}}. \quad \text{(A3)}$$

Because $\beta(\alpha, \lambda)$ for water molecules is given by Morel[41] and its angular distribution is considered to be wavelength independent for the visible region, the above equation can be simplified to

$$Q_m^{\text{sun}}(j) \approx 5.92 - 3.05\cos(j). \quad \text{(A4)}$$

As backscattered skylight also contributes to the upwelling-radiance field, its influence on the actual $Q_m(j, \lambda)$ needs to be considered. Defining the ratio between the subsurface, downwelling sky irradiance and solar irradiance to be $\gamma(\lambda)$ and assuming that the Q factor that is due to skylight is ~ 3.14, we have

$$Q_m(j, \lambda) = \frac{1 + \gamma(\lambda)}{1 + \gamma(\lambda)\frac{Q_m^{\text{sun}}(j)}{3.14}}Q_m^{\text{sun}}(j). \quad \text{(A5)}$$

So, for molecular scattering and when j and $\gamma(\lambda)$ are known for any station, $Q_m(j, \lambda)$ can be estimated.

Appendix B: Remote-Sensing Reflectance for CDOM Fluorescence and Water Raman

For z positive downward from the surface, Θ the zenith angle, and ϕ the azimuthal angle, with the consideration of isotropic β_{ie}, to the first order, the inelastic radiance $L_{u,ie}$ in the direction Θ and the upwelling irradiance $E_{u,ie}$ at depth z resulting from the depth interval dz are simplified to

$$dL_{u,ie}(z, \theta, \lambda) = \int_{\lambda_x}\beta_{ie}(\lambda_x, \lambda)E_0(z, \lambda_x)d\lambda_x\frac{dz}{\cos(\theta)}, \quad \text{(B1)}$$

and

$$dE_{u,ie}(z, \lambda) = 2\pi\int_{\pi/2}^{\pi}dL_{u,ie}(z, \theta, \lambda)\cos(\theta)\sin(\theta)d\theta = 2\pi\int_{\lambda_x}\beta_{ie}(\lambda_x, \lambda)E_o(z, \lambda_x)d\lambda_x dz, \quad \text{(B2)}$$

where $E_o(z, \lambda_x)$ is the scalar irradiance at depth z, and $E_o(z, \lambda_x) = E_{od}(z, \lambda_x) + E_{ou}(z, \lambda_x) \approx D_d(1 + 2R(\lambda_x))E_d(z, \lambda_x)$. Consider that $R(\lambda_x)$ is small (<0.05) and $D_u/D_d(\approx 2)$[20] is independent of depth, the subsurface irradiance resulting from the inelastic scattering for a deep water column is

$$E_{u,ie}(0^-, \lambda) \approx 2\pi\int_{\lambda_x}\frac{\beta_{ie}(\lambda_x, \lambda)E_d(0^-, \lambda_x)}{2\kappa(\lambda) + \kappa(\lambda_x)}d\lambda_x. \quad \text{(B3)}$$

If one defines Q_{ie} as the Q factor for the inelastic-scattering field, then the subsurface upwelling radiance caused by inelastic scattering is

$$L_{u,ie}(0^-, \lambda) \approx \frac{2\pi}{Q_{ie}}\int_{\lambda_x}\frac{\beta_{ie}(\lambda_x, \lambda)E_d(0^-, \lambda_x)}{2\kappa(\lambda) + \kappa(\lambda_x)}d\lambda_x. \quad \text{(B4)}$$

The inelastic total scattering coefficient $\psi(\lambda_x, \lambda)$ (m^{-1}/nm) is defined as

$$\psi(\lambda_x, \lambda) = \int_{4\pi}\beta_{ie}(\alpha, \lambda_x, \lambda)d\omega. \quad \text{(B5)}$$

Because $\beta_{ie}(\alpha, \lambda_x, \lambda)$ is considered isotropic, then

$$\psi(\lambda_x, \lambda) = 4\pi\beta_{ie}(\lambda_x, \lambda). \quad \text{(B6)}$$

According to the definition of remote-sensing reflectance and with Eqs. (B4) and (B6), we have

$$R_{rs,ie}(\lambda) \approx \frac{I}{2Q_{ie}}\int_{\lambda_x}\frac{\psi(\lambda_x, \lambda)E_d(0^-, \lambda_x)}{[2\kappa(\lambda) + \kappa(\lambda_x)]E_d(0^-, \lambda)}d\lambda_x. \quad \text{(B7)}$$

For CDOM fluorescence, if $\eta(\lambda_x)$ is defined as the quantum efficiency for the emission band excited by

λ_x, then[9,16]

$$\eta(\lambda_x) = \int_\lambda \frac{\lambda}{\lambda_x} \frac{\psi(\lambda_x, \lambda)}{a_g(\lambda_x)} d\lambda. \quad \text{(B8)}$$

$\psi(\lambda_x, \lambda)$ can be characterized by a log-normal curve,[33] so

$$\psi(\lambda_x, \lambda) = \frac{\eta(\lambda_x)\lambda_x a_g(\lambda_x)}{\lambda A} \exp\left[-s\left(\ln\frac{\lambda - \lambda_0}{\sigma}\right)^2\right] \quad \text{(B9)}$$

in which

$$A = \int_\lambda \exp\left[-s\left(\ln\frac{\lambda - \lambda_0}{\sigma}\right)^2\right] d\lambda, \quad \text{(B10)}$$

where $\eta(\lambda_x)$, λ_0, s, and σ may vary with the type of CDOM and λ_x.

In general, $b_b \ll a$ for most oceanic waters,[21] so κ is close to a, and based on the calculation for chl a fluorescence made by Gordon[16] the Q_{ie} factor for inelastic scattering is ~ 3.7. Then combining Eqs. (B7) and (B9), the remote-sensing reflectance caused by CDOM fluorescence can be reduced to

$$R_{rs}^f(\lambda) \approx 0.072 \int_{\lambda_x} \eta(\lambda_x) \frac{\lambda_x}{\lambda} \frac{a_g(\lambda_x)E_d(0^-, \lambda_x)}{[2a(\lambda) + a(\lambda_x)]E_d(0^-, \lambda)} \times \frac{\exp\left[-s\left(\ln\frac{\lambda - \lambda_0}{\sigma}\right)^2\right]}{A} d\lambda_x. \quad \text{(B11)}$$

Unlike broadband (~ 100 nm) CDOM fluorescence, the water Raman emission has a half bandwidth of approximately 20 nm.[32] If this bandwidth, is omitted, i.e., a narrow Raman emission is assumed, the inelastic-scattering coefficient $\psi(\lambda_x, \lambda)$ for water Raman can be related to the Raman scattering coefficient as

$$\psi(\lambda_x, \lambda)d\lambda_x = b_R(\lambda_x),$$

and from Eq. (B7), with $\kappa \approx a$, the remote-sensing reflectance for water Raman is

$$R_{rs}^R(\lambda) \approx 0.072 \frac{b_R(\lambda_x)E_d(0^-, \lambda_x)}{[2a(\lambda) + a(\lambda_x)]E_d(0^-, \lambda)}. \quad \text{(B12)}$$

Financial support was provided by NASA through grant NAGW–465 and Goddard Space Flight Center contract NAS5–30779, and by the Office of Naval Research through grant N00014–89–J–1091. Some ship support was provided by the State of Florida through the Florida Institute of Oceanography. The authors thank B. Chen and J. Hesler for administrative assistance.

References

1. H. R. Gordon, D. K. Clark, J. L. Mueller, and W. A. Hovis, "Phytoplankton pigments from the Nimbus-7 Coastal Zone Color Scanner: comparisons with surface measurements," Science **210,** 63–66 (1980).
2. K. L. Carder, R. G. Steward, J. H. Paul, and G. A. Vargo, "Relationships between chlorophyll and ocean color constituents as they affect remote-sensing reflectance models," Limnol. Oceanogr. **31,** 403–413 (1986).
3. A. Morel, "Optical modeling of the upper ocean in relation to its biogenous matter content (case 1 waters)," J. Geophys. Res. **93,** 10,749–10,768 (1988).
4. K. L. Carder, W. W. Gregg, D. K. Costello, K. Haddad, and J. M. Prospero, "Determination of Saharan dust radiance and chlorophyll from CZCS imagery," J. Geophys. Res. **96,** 5369–5378 (1991).
5. A. Morel and J. M. Andre, "Pigment distribution and primary production in the western Mediterranean as derived and modeled from Coastal Zone Color Scanner observations," J. Geophys. Res. **96,** 12,685–12,698 (1991).
6. K. L. Carder, S. K. Hawes, K. A. Baker, R. C. Smith, R. G. Steward, and B. G. Mitchell, "Reflectance model for quantifying chlorophyll a in the presence of productivity degradation products," J. Geophys. Res. **96,** 20,599–20,611 (1991).
7. T. Platt, C. Caverhill, and S. Sathyendranath, "Basic-scale estimates of oceanic primary production by remote sensing: the North Atlantic," J. Geophys. Res. **96,** 15,147–15,159 (1991).
8. S. Sathyendranath, L. Prieur, and A. Morel, "A three-component model of ocean colour and its application to remote sensing of phytoplankton pigments in coastal waters," Int. J. Remote Sensing **10,** 1373–1394 (1989).
9. K. L. Carder and R. G. Steward, "A remote-sensing reflectance model of a red tide dinoflagellate off West Florida," Limnol. Oceanogr. **30,** 286–298 (1985).
10. H. R. Gordon, O. B. Brown, R. H. Evans, J. W. Brown, R. C. Smith, K. S. Baker, and D. K. Clark, "A semianalytic radiance model of ocean color," J. Geophys. Res. **93,** 10,909–10,924 (1988).
11. T. G. Peacock, K. L. Carder, C. O. Davis, and R. G. Seward, "Effects of fluorescence and water Raman scattering on models of remote-sensing reflectance," in *Ocean Optics X,* R. W. Spinrad, ed., Proc. Soc. Photo-Opt. Instrum. Eng. **1302,** 303–319 (1990).
12. R. W. Austin, "Inherent spectral radiance signatures of the ocean surface," in *Ocean Color Analysis (Final Technical Report),* S. Q. Duntley, ed., SIO ref. 74–10 (Scripps Institution of Oceanography, La Jolla, Calif., 1974), pp. 2.1–2.20.
13. F. C. Polcyn, W. L. Brown, and I. J. Sattinger, "The measurement of water depth by remote-sensing techniques," Rep. 8973–26–F (Willow Run Laboratories, University of Michigan, Ann Arbor, Mich., 1970).
14. R. K. Clark, T. H. Fay, and C. L. Walker, "Bathymetry calculations with Landsat 4 TM imagery under a generalized ratio assumption," Appl. Opt. **26,** 4036–4038 (1987).
15. D. R. Lyzenga, "Passive remote-sensing techniques for mapping water depth and bottom features," Appl. Opt. **17,** 379–383 (1978).
16. H. R. Gordon, "Diffuse reflectance of the ocean: the theory of its augmentation by chl a fluorescence at 685 nm," Appl. Opt. **18,** 1161–1166 (1979).
17. C. S. Yentsch and D. A. Phinney, "Spectral fluorescence: an ataxonomic tool for studying the structure of phytoplankton populations," J. Plankton Res. **7,** 617–632 (1985).
18. H. R. Gordon, "Modeling and simulating radiative transfer in the ocean," in *Ocean Optics,* R. W. Spinrad, K. L. Crader, and M. J. Perry, eds., Oxford Monogr. Geol. Geophys. No. 25 (Oxford U. Press, New York, 1994), pp. 3–39.
19. J. P. Riley and R. Chester, *Introduction to Marine Chemistry,* (Academic, London, 1971), Chap. 2, p. 17.

20. H. R. Gordon, O. B. Brown, and M. M. Jacobs, "Computed relationship between the inherent and apparent optical properties of a flat homogeneous ocean," Appl. Opt. **14,** 417–427 (1975).
21. A. Morel and L. Prieur, "Analysis of variations in ocean color," Limnol. Oceanogr. **22,** 709–722 (1977).
22. J. T. O. Kirk, "Volume scattering function, average cosines, and the underwater light field," Limnol. Oceanogr. **36,** 455–467 (1991).
23. J. T. O. Kirk, "Dependence of relationship between inherent and apparent optical properties of water on solar altitude," Limnol. Oceanogr. **29,** 350–356 (1984).
24. A. Morel and B. Gentili, "Diffuse reflectance of oceanic waters: its dependence on sun angle as influenced by the molecular scattering contribution," Appl. Opt. **30,** 4427–4438 (1991).
25. H. R. Gordon, "Dependence of the diffuse reflectance of natural waters on the sun angle," Limnol. Oceanogr. **34,** 1484–1489 (1989).
26. B. R. Marshall and R. C. Smith, "Raman scattering and in-water ocean properties," Appl. Opt. **29,** 71–84 (1990).
27. K. L. Crader, P. Reinersman, R. F. Chen, F. Muller-Karger, C. O. Davis, and M. Hamilton, "AVIRIS calibration and application in coastal oceanic environments," Remote Sens. Environ. **44,** 205–216 (1993).
28. B. G. Mitchell and D. A. Kiefer, "Chl *a* specific absorption and fluorescence excitation spectra for light limited phytoplankton," Deep-Sea Res. **35,** 635–663 (1988).
29. A. Bricaud and D. Stramski, "Spectral absorption coefficients of living phytoplankton and nonalgal biogenous matter: A comparison between the Peru upwelling area and the Sargasso Sea," Limnol. Oceanogr. **35,** 562–582 (1990).
30. R. C. Smith and K. S. Baker, "Optical properties of the clearest natural waters," Appl. Opt. **20,** 177–184 (1992).
31. R. H. Stavn and A. D. Weidemann, "Optical modeling of clear ocean light fields: Raman scattering effects," Appl. Opt. **27,** 4002–4011 (1988).
32. D. J. Collins, J. A. Bell, R. Zanoni, I. S. McDermid, J. B. Breckinridge, and C. A. Sepulveda, "Recent progress in the measurement of temperature and salinity by optical scattering," in *Ocean Optics VII (Monterey),* M. A. Blizard, ed., Proc. Soc. Photo-Opt. Instrum. Eng. **489,** 247–269 (1984).
33. S. K. Hawes, K. L. Carder, and G. R. Harvey, "Quantum fluorescence efficiencies of marine humic and fulvic acids: effects on ocean color and fluorometric detection," *Ocean Optics XI,* G. D. Gilbert, ed., Proc. Soc. Photo-Opt. Instrum. Eng. **1750,** 212–223 (1992).
34. National Oceanic and Atmospheric Administration, Provisional Chart No. 1003, United States: Gulf Coast and Key West to the Mississippi River (National Oceanic and Atmospheric Administration, Washington, D.C., 1972).
35. H. R. Gordon and A. Morel, *Remote Assessment of Ocean Color for Interpretation of Satellite Visible Imagery: A Review* (Springer-Verlag, New York, 1983), p. 44.
36. R. W. Austin, "Coastal zone color scanner radiometry," *Ocean Optics VI (Monterey),* S. Q. Duntley, ed., Proc. Soc. Photo-Opt. Instrum. Eng. **208,** (1979). 170–177.
37. J. T. O. Kirk, *Light and Photosynthesis in Aquatic Ecosystems.* (Cambridge U. Press, London, 1986), Chap. 6, p. 117.
38. C. O. Davis, Jet Propulsion Laboratory, Pasadena, Calif. 91109 (personal communication, August 1992).
39. A. Morel and B. Gentili, "Diffuse reflectance of oceanic waters (2): Bi-directional aspects," Appl. Opt. **32,** 6864–6879 (1993).
40. N. G. Jerlov, *Optical Oceanography,* Vol. 5 of Elsevier Oceanography Series (Elsevier, New York, 1968), pp. 81–84.
41. A. Morel, "Optical properties of pure water and pure sea water," in *Optical Aspects of Oceanography,* N. G. Jerlov and E. S. Nielsen, eds. (Academic, New York, 1974), pp. 1–24.
42. W. W. Gregg and K. L. Crader, "A simple spectral solar irradiance model for cloudless maritime atmospheres," Limnol. Oceanogr. **35,** 1657–1675 (1990).
43. A. Morel and Y. H. Ahn, "Optical efficiency factors of free-living marine bacteria: influence of bacterioplankton upon the optical properties and particulate organic carbon in oceanic waters," J. Mar. Res. **48,** 145–175 (1990).
44. A. Bricaud and A. Morel, "Light attenuation and scattering by phytoplanktonic cells: a theoretical modeling," Appl. Opt. **25,** 571–580 (1986).
45. D. Spitzer and R. W. J. Dirks, "Contamination of the reflectance of natural waters by solar-induced fluorescence of dissolved organic matter," Appl. Opt. **24,** 444–445 (1985).
46. R. H. Stavn, "Raman scattering effects at the shorter visible wavelengths in clear ocean waters," in *Ocean Optics X,* R. W. Spinrad, ed., Proc. Soc. Photo-Opt. Instrum. Eng. **1302,** 94–100 (1990).
47. C. S. Yentsch and C. M. Yentsch, "Fluorescence spectral signatures: the characterization of phytoplankton populations by the use of excitation and emission spectra," J. Mar. Res. **37,** 471–483 (1979).
48. A. C. Tam and C. K. N. Patel, "Optical absorptions of light and heavy water by laser optoacoustic spectroscopy," Appl. Opt. **18,** 3348–3358 (1979).